# Proteasomes Associated with the Blm10 Activator Protein Antagonize Mitochondrial Fission through Degradation of the Fission Protein Dnm1*

**Krisztina Tar**[‡1], **Thomas Dange**[‡1], **Ciyu Yang**[‡], **Yanhua Yao**[‡], **Anne-Laure Bulteau**[§], **Elena Fernandez Salcedo**[‡], **Stephen Braigen**[‡], **Frederic Bouillaud**[§], **Daniel Finley**[¶], and **Marion Schmidt**[‡2]

From the ‡Department of Biochemistry, Albert Einstein College of Medicine, Bronx, New York 10461, §INSERM, Institute Cochin, 24 Rue du Faubourg Saint Jacques, 75014 Paris, France, and the ¶Department of Cell Biology, Harvard Medical School, Boston, Massachusetts 10115

**Background:** Blm10 binds to the proteasome core particle and stimulates its proteolytic activity.
**Results:** Loss of *BLM10* results in impaired respiration, elevated oxidative stress sensitivity, increased mitochondrial fission, and stabilization of the fission protein Dnm1.
**Conclusion:** Blm10 proteasome-mediated Dnm1 degradation is a regulatory mechanism to maintain correct mitochondrial function.
**Significance:** Blm10 is involved in mitochondrial quality control under oxidative stress.

The conserved Blm10/PA200 activators bind to the proteasome core particle gate and facilitate turnover of peptides and unfolded proteins *in vitro*. We report here that Blm10 is required for the maintenance of functional mitochondria. *BLM10* expression is induced 25-fold upon a switch from fermentation to oxidative metabolism. In the absence of *BLM10*, *Saccharomyces cerevisiae* cells exhibit a temperature-sensitive growth defect under oxidative growth conditions and produce colonies with dysfunctional mitochondria at high frequency. Loss of *BLM10* leads to reduced respiratory capacity, increased mitochondrial oxidative damage, and reduced viability in the presence of oxidative stress or death stimuli. In the absence of *BLM10*, increased fragmentation of the mitochondrial network under oxidative stress is observed indicative of elevated activity of the mitochondrial fission machinery. The degradation of Dnm1, the main factor mediating mitochondrial fission, is impaired in the absence of *BLM10 in vitro* and *in vivo*. These data suggest that the mitochondrial functional and morphological changes observed are related to elevated Dnm1 levels. This hypothesis is supported by the finding that cells that constitutively overexpress *DNM1* display the same mitochondrial defects as *blm10Δ* cells. The data are consistent with a model in which Blm10 proteasome-mediated turnover of Dnm1 is required for the maintenance of mitochondrial function and provides cytoprotection under conditions that induce increased mitochondrial damage and programmed cell death.

The proteasome is the major proteolytic system in the cytoplasm and nuclei of eukaryotic cells (1). It is required for the maintenance of protein homeostasis through its ability to eliminate damaged and misfolded proteins. Furthermore, its activity is vital for numerous cellular processes that are regulated by the temporally specific degradation of pathway components (1). Because the proteasome provides building blocks for protein synthesis, it also has a metabolic function under nutrient-limiting conditions (2).

Proteasomal activity is subject to tight regulation. The central regulatory mechanism is defined by the topology of its proteolytic core complex, the core particle (CP[3] or 20 S proteasome). The barrel-shaped structure of the CP is formed by four stacked rings, which sequester the proteolytic sites within the interior chamber (3). Access to the degradation chamber is regulated by adjustable gates, located at both ends of the cylinder (4). To promote substrate degradation, the CP must interact with proteasome activators, which open the gate, thus allowing substrate entry (5). To date, three types of proteasome activators are known as follows: the conserved regulatory particle (RP/19S/PA700) (6, 7); activators of the PA28 protein family present in higher eukaryotes (8), and the conserved Blm10/PA200 activator family (9, 10). The RP is required for the ATP-dependent unfolding and degradation of ubiquitinated proteasome substrates. PA28 activators mediate ATP- and ubiquitin-independent turnover of specific proteasome substrates (11, 12). As RP and PA28 activators, Blm10/PA200 proteins enhance the proteasomal peptidase activity (9, 10, 13, 14) and accelerate the degradation of substrates with intrinsically disordered domains such as Tau (14) or acetylated histones (15) in the absence of ATP or ubiquitin, similar to the activity of PA28

[3] The abbreviations used are: CP, core particle; RP, regulatory particle; UPS, ubiquitin-proteasome system; CHX, cycloheximide; CCCP, carbonyl cyanide *m*-chlorophenylhydrazone; TET, triethyltin bromide; RSV, respiratory state value; PDS, post-diauxic shift; YP/D, yeast peptone dextrose.

proteins (11, 12). Blm10 has also been associated with proteasome holocomplex formation (16, 17).

In yeast and in mammalian cells, Blm10/PA200 proteasomes form a substantial proteasome subpopulation, where the CP/20 S cylinder is flanked on one side with Blm10/PA200 and with RP/19S on the opposite side (10, 18). Blm10 proteasome-mediated turnover is involved in the transcriptional down-regulation of ribosome biosynthesis in response to nutrient depletion through degradation of the ribosome-related transcription factor Sfp1 (19). Loss of PA200 in mice results in defective spermatogenesis (15, 20), and the protein is recruited to chromatin upon $\gamma$-irradiation-induced DNA damage (15, 18). PA200 also plays a role in the maintenance of glutamine/glutamate homeostasis in mammalian cells (21). In addition, overexpression of *BLM10* in yeast causes growth defects on nonfermentable carbon sources at elevated temperatures (14); recently, increased frequency of cells with dysfunctional mitochondria in cells lacking *BLM10* was reported (22). These observations indicate that the cellular functions of Blm10/PA200 proteasomes might be related to the regulation of metabolic adaptation and stress response.

The ubiquitin proteasome system (UPS) has been implicated in the maintenance of mitochondrial structural dynamics and homeostasis. The E3 ubiquitin ligase Rsp5 is required for correct mitochondrial inheritance during vegetative growth (23), and proteasomal inhibition *in vivo* results in the ubiquitination and accumulation of a model substrate located in the mitochondrial intermembrane space (24). Additional reports demonstrate proteasome-mediated degradation of proteins, which associate with the outer mitochondrial membrane (25). These findings support a model in which the proteasome provides a protein quality control function for mitochondrial proteins. A particular mitochondrion-related function mediated by the UPS is the regulation of mitochondrial dynamics. In most eukaryotic cells, mitochondria form a dynamic network and are subject to continuous fission and fusion. Unopposed fission or fusion in response to deletion of the specific factors involved results in a reduction of mitochondrial functionality (26). The fusion of mitochondria promotes repair and complementation processes to optimize the respiratory capacity of the organelle (27), whereas damaged mitochondria are segregated from the network by fission, promoting mitophagy (28). Thus, mitochondrial fission and fusion are thought to provide an organellar quality control mechanism.

A screen for mitochondrial morphological defects upon down-regulation of essential genes in yeast revealed that loss of individual proteasome subunits leads to altered mitochondrial morphology (29). Altered mitochondrial morphology was also observed for mutants of proteasome RP subunits, surprisingly with the following opposite outcome: mutations in *RPN11* result in fragmented mitochondria (30, 31), whereas an *RPN3* mutant exhibits fused mitochondria (31). It is assumed that the underlying mechanism for altered mitochondrial morphology in proteasome mutants is related to proteasome-mediated turnover of Fzo1/mitofusin, a mitochondrial fusion protein (32–34).

In this study, we provide evidence for an additional regulatory function of the proteasome in mitochondrial homeostasis, mediated by the proteasome activator Blm10. In the absence of *BLM10*, a high frequency of colonies with dysfunctional mitochondria is observed, and the cells display a temperature-dependent growth defect under conditions that require functional mitochondria. Mitochondria isolated from *blm10*$\Delta$ cells exhibit reduced respiratory activity and increased oxidative damage. Consistent with these findings, we observed decreased viability in the absence of *BLM10* after exposure to oxidizing reagents such as hydrogen peroxide and menadione. In the presence of oxidative stress, cells lacking *BLM10* exhibit increased mitochondrial fragmentation. The primary protein, which drives mitochondrial fragmentation, is Dnm1. Loss of *BLM10* leads to Dnm1 stabilization, and overexpressing *DNM1* phenocopied the mitochondrial functional and structural changes of *blm10*$\Delta$ cells. These data argue for a model in which the regulated turnover of Dnm1 mediated by Blm10 proteasomes is required for normal mitochondrial function and under oxidative stress. Mitochondrial fragmentation is also an integral mechanism of programmed cell death/apoptosis, and changes in Dnm1 activity affect the cellular response to death stimuli (28, 35). In agreement with Blm10 proteasome-mediated regulation of Dnm1 abundance, we find that loss of *BLM10* confers hypersensitivity to hydrogen peroxide or to high doses of acetic acid. Finally, we demonstrate that the impact of Blm10 on mitochondrial dynamics requires proteasome interaction, because a *BLM10* mutation that abrogates CP binding recapitulates the effects of *BLM10* deletion. The impact of Blm10 on Dnm1 abundance is also evident from *in vitro* studies, which demonstrate that Blm10 mediates proteasomal turnover of Dnm1. Our data indicate that Blm10 proteasome-mediated degradation of Dnm1 is a regulatory mechanism to counteract mitochondrial fission and provides a cytoprotective function under conditions that induce mitochondrial stress.

## EXPERIMENTAL PROCEDURES

*Strains, Media, Growth Conditions, and Chemicals*—All strains and plasmids used in this work are listed in Tables 1 and 2, respectively. They were obtained using standard genetic techniques. All strains are isogenic to BY4741 or BY4742 (36) and are S288C-derived. Complete gene deletion, promoter exchange, or tag integration was performed at the genomic locus by homologous recombination using standard techniques (37). Primer sequences are available upon request. Unless otherwise noted, strains were grown at 30 °C in yeast peptone/dextrose (YPD) and were harvested at $OD_{660\,nm}$ ~1 for log phase cells, at $OD_{660\,nm}$ ~12 for PDS phase cells, and after 5 days for stationary phase cells. Cycloheximide (CHX), hydrogen peroxide, menadione, and acetic acid were purchased from Sigma.

*Phenotypic Analysis*—To quantify the frequency of petite colonies, strains were grown in YPD overnight, harvested, diluted to ~100 cells per plate and spread onto YPD plates. Petite frequency was determined after 48 h by visual inspection. To confirm that petite colony formation originates from mitochondrial dysfunction, normal and petite colonies were grown on YP/glycerol plates containing 3% glycerol. For phenotypic analysis, strains were grown overnight in YPD and diluted in 96-well plates to a density of $6 \times 10^6$ cells per well followed by

## TABLE 1
### Strains used in this study

| Strains | Genotypes | Source |
|---|---|---|
| BY4741 | *MATa his3Δ1 leu2Δ0 met15Δ0 ura3Δ0* | 34 |
| BY4742 | *MATα his3Δ1 leu2Δ0 lys2Δ0 ura3Δ0* | 34 |
| yMS63 | *MATa his3Δ1 leu2Δ0 met15Δ0 ura3Δ0 blm10Δ::NatMX* | 18 |
| yMS76 | *MATa his3Δ1 leu2Δ0 met15Δ0 ura3Δ0 blm10Δ::NatMX + pOK29-COX4-GFP* | This study |
| yMS118 | *MATa his3Δ1 leu2Δ0 met15Δ0 ura3Δ0 blm10Δ::NatMX + yCplac111GFP-BLM10* | This study |
| yMS131 | *MATa his3Δ1 leu2Δ0 met15Δ0 ura3Δ0 blm10Δ::NatMX* | This study |
| yMS268 | *MATα his3Δ1 leu2Δ0 met15Δ0 lys2Δ0 ura3Δ0* | 18 |
| yMS285 | *MATα his3Δ1 leu2Δ0 ura3Δ0 rpn4Δ::KanMX* | This study |
| yMS567 | *MATa his3Δ1 leu2Δ0 met15Δ0 ura3Δ0 blm10ΔC3::KanMX* | 18 |
| yMS713 | *MATa his3Δ1 leu2Δ0 met15Δ0 lys2Δ0 ura3Δ0 fis1Δ::KanMX* | This study |
| yMS794 | *MATa his3Δ1 leu2Δ0 met15Δ0 lys2Δ0 ura3Δ0 dnm1Δ::HphMX* | This study |
| yMS1058 | *MATα his3Δ1 leu2Δ0 lys2Δ0 ura3Δ0 (NatMX)TEFpDNM1* | This study |
| yMS1060 | *MATa his3Δ1 leu2Δ0 met15Δ0 ura3Δ0 dnm1Δ::HphMX + pOK29-COX4-GFP* | This study |
| yMS1539 | *MATa his3Δ1 leu2Δ0 lys2Δ0 ura3Δ0 + pGREG586-His₆-DNM1* | This study |
| yMS1731 | *MATα MATα his3Δ1 leu2Δ0 met15Δ0 lys2Δ0 ura3Δ0 blm10Δ::NatMX ((NatMX)TEFpDNM1)* | This study |
| yMS1798 | *MATa his3Δ1 leu2Δ0 met15Δ0 lys2Δ0 ura3Δ0 (NatMX)TEFpDNM1 + pCOX4-GFP* | This study |
| yMS1849 | *MATa his3Δ1 leu2Δ0 met15Δ0 ura3Δ0 blm10Δ::NatMX dnm1Δ::HphMX + pCOX4-GFP* | This study |
| yMS1942 | *MATa his3Δ1 leu2Δ0 met15Δ0 ura3Δ0 + pOK29-COX4-GFP* | This study |
| yMS1943 | *MATa his3Δ1 leu2Δ0 met15Δ0 ura3Δ0 blm10ΔC3::KanMX + pOK29-COX4-GFP* | This study |
| yMS2092 | *MATa his3Δ1 leu2Δ0 met15Δ0 ura3Δ0 FZO1-HA3 (HIS3)* | This study |
| yMS2093 | *MATa his3Δ1 leu2Δ0 met15Δ0 ura3Δ0 blm10Δ::NatMX FZO1-HA3 (HIS3)* | This study |
| yMS2094 | *MATa his3Δ1 leu2Δ0 met15Δ0 ura3Δ0 blm10ΔC3::KanMX FZO1-HA3 (HIS3)* | This study |
| yMS2096 | *MATa his3Δ1 leu2Δ0 met15Δ0 ura3Δ0 rpn4Δ:: HphMX FZO1-HA3 (HIS3)* | This study |

## TABLE 2
### Plasmids used in this study

| Plasmid | Source |
|---|---|
| yCPLac111-*GFP-BLM10* | This study |
| pGREG586-*His₆-DNM1* | This study |
| pOK29 -*COX4-GFP* | 37 |

5-fold serial dilutions. They were spotted onto solid media, and colony growth was monitored. Carbon sources in the complete media used were as follows: YPD, 2% glucose; YP/acetate, 0.1 M acetate; and YP/glycerol, 3% glycerol. To analyze survival after oxidative stress, logarithmically growing cells were treated with 10 mM $H_2O_2$ or 300 $\mu$M menadione for 3.5 or 1.5 h, respectively, prior to spotting onto solid YPD medium.

*Quantitative Real Time PCR*—Total RNA was isolated from WT cells grown in YP/glycerol for the time indicated by acidic phenol/chloroform extraction. Subsequently, 1 $\mu$g of RNA was treated with DNase (Invitrogen), followed by reverse transcription using the High Capacity cDNA kit (Applied Biosystems). Primers were designed using the software Primer3Plus. The sequences are available upon request. cDNA from 1 $\mu$g of RNA was subjected to quantitative RT-PCR using the SYBR Green PCR Master Mix (Applied Biosystems) in an IQ5 Bio-Rad real time PCR detection system. The reactions were performed in 40 cycles at 95 °C for 30 s, 58 °C for 30 s, and 72 °C for 40 s after an initial activation at 95 °C for 2 min. Negative controls were run simultaneously for each reaction. Data were analyzed using the IQ5 Optical System software. To compare the relative mRNA expression between the individual genes and the endogenous reference gene *ACT1*, the comparative threshold cycle ($C_T$) method was used. The amount of target, relative to the reference gene as described in the figure legends, is given by $2 - \Delta\Delta C_T$. All reactions were performed in triplicate. Error bars indicate the mean ± S.E. of three independent experiments.

*Respiration Assay*—The oxygen consumption of WT or *blm10Δ* cells was measured at 30 °C using an Oroboros instrument (Oroboros, Graz, Austria). Respiratory rates (*JO*) were determined from the slope of a plot of $O_2$ concentration *versus* time. For all assays, 2 ml of growing cell suspension were used. Respiration assays of growing cells were performed in the growth medium plus 2% lactate when triethyltin bromide (TET) (Sigma) was added at 0.2 mM and carbonyl cyanide *m*-chlorophenylhydrazone (CCCP) (Sigma) at 10 $\mu$M. Respiratory state value (RSV) is defined as $(JO_{2basal} - JO_{2TET})/(JO_{2CCCP} - JO_{2TET})$. RSV represents the percentage of stimulation of oxidative phosphorylation compared with the basal respiration capacity (38).

*Isolation of Yeast Mitochondria*—Yeast cells were cultured overnight at 30 °C in YP/lactate medium) and harvested by centrifugation at 4,000 × g for 10 min at 4 °C, washed with 50 ml of ice-cold water, and resuspended in 0.6 M sorbitol, 50 mM Tris-HCl, pH 7.5, supplemented with complete protease inhibitor mixture (Sigma). 4 ml of 0.45-mm diameter sterile glass beads were added to each tube, and the cells were lysed by vortexing six times for 30 s each, at 2-min intervals, on ice. All subsequent steps were carried out at 4 °C. Glass beads and unbroken cells were removed by centrifugation at 4,000 × g for 10 min; supernatants were centrifuged (14,000 × g, 10 min, 4 °C), and the resulting pellets containing mitochondria were resuspended in 0.6 M sorbitol, 50 mM Tris-HCl, pH 7.5.

*Aconitase Activity Assay*—Mitochondria were diluted to 0.05 mg/ml in 25 mM $KH_2PO_4$, pH 7.25, containing 0.05% Triton X-100. Aconitase activity was assayed as the rate of NADP reduction (340 nm, $\epsilon = 6200$ $M^{-1}$ $cm^{-1}$) by isocitrate dehydrogenase upon addition of 1.0 mM sodium citrate, 0.6 mM $MnCl_2$ (a cofactor of isocitrate dehydrogenase), 0.2 mM NADP, and 1.0 unit/ml isocitrate dehydrogenase to solubilized mitochondria (0.05 mg/ml mitochondrial protein). Isocitrate dehydrogenase (Sigma) was exchanged into a buffer composed of 25 mM $KH_2PO4$, pH 7.25, by gel filtration (PD-10 column, GE Healthcare) prior to incubations. Use of oxalomalate (2.0 mM), a competitive inhibitor of aconitase, ensured the specificity of the assay.

*Live Cell Fluorescence Microscopy*—To visualize mitochondria, mitochondrially targeted pCox4-GFP (pOK29) (39) was introduced into the strains indicated via transformation. Blm10

localization during the fermentative phase of yeast growth (log) or after the switch to oxidative metabolism (PDS) was determined using a plasmid with an N-terminal *BLM10* GFP fusion (yCPLac111-*GFP-BLM10*) under the endogenous promoter in *blm10Δ* cells. Live cell fluorescence was monitored using a fluorescence microscope (Olympus BX61) at the Albert Einstein Imaging Facility with a ×60 or ×100 NA 1.4 objective (PlanApo). Fluorescence or differential interference contrast images were captured with a cooled CCD camera (Sensicam QE) using IPlab 4.0 software. Images were identically processed using ImageJ software 1.42q. For excitation of GFP, a 450–490-nm bandpass filter was used. Emitted light was detected with a 520-nm long pass filter (filter set Olympus).

*Detection of Steady State Protein Levels*—Cells from WT and mutant strains were harvested in the respective growth phases and stored at −80 °C. Cells were disrupted by alkaline lysis as described previously (19). Protein concentration was determined using a Bradford protein assay (Bio-Rad). Equal protein amounts were subjected to SDS-PAGE and immunodetection. Antibodies used were anti-Dnm1, anti-Fis1, and anti-Mdv1 (kindly provided by Janet Shaw). Anti-phosphoglycerate kinase 1 (Pgk1) (Invitrogen) was used as a loading control. To investigate Fzo1 levels, the protein was C-terminally tagged with $HA_3$ at the genomic locus in the strains indicated. Anti-HA antibodies (Roche Applied Science) were used for Fzo1 detection. Immunoblot signals were detected via enhanced chemiluminescence (ECL) using a kit (Pierce). For quantification, signals were recorded using an ImageQuant LAS4000 mini system (GE Healthcare). The band intensity was quantified using the ImageQuant TL software (GE Healthcare).

*In Vivo Protein Degradation Assay*—Protein turnover in wild type (WT), *blm10Δ*, *blm10ΔC3*, and *rpn4Δ* strains (BY4741, yMS63, yMS567, and yMS285, respectively) was determined via a CHX chase. To analyze proteasome-dependent degradation, log phase cultures were supplemented with lethal doses of the translation inhibitor CHX at 0.2 mg/ml (Sigma). Aliquots were harvested at the times indicated and subjected to alkaline lysis. Equal protein amounts were subjected to SDS-PAGE and to immunodetection using anti-Dnm1, anti-Fis1, or anti-Mdv1 antibodies. Detection of phosphoglycerate kinase 1 (PGK1) was used as a loading control. Signals were detected via enhanced chemiluminescence (ECL) using a kit (Pierce). For quantification, the chemiluminescence of the bands was recorded using an ImageQuant LAS4000 mini system (GE Healthcare). The band intensity was quantified using the ImageQuant TL software (GE Healthcare).

*Protein Purification*—To construct a vector for Dnm1 purification from yeast, the *DNM1* gene was amplified from yCPLacIII-Dnm1 plasmid, which was obtained via gapped repair, with the following primers: Rec1_F_Dnm1, 5′GAATTCGATATCAAGCTTTATGCATACCGTCGACAATGGCTAGTTTAGAAGATCTTATTCCTACT3′; Rec2_R_Dnm1: 5′GCGTGACATAACTAATTACATGACTCGAGGTCGACTTACAGAATA**TT**ACTAATAAGGGGTTGCAGCCTT3′.

The gene was subcloned into pGREG586 containing a galactose-inducible N-terminal $His_6$ tag via homologous recombination (40). The resulting vector pGREG586-$His_6$-*DNM1* was verified by sequencing and transformed into a WT strain to

create yMS1539. The strain was grown overnight in synthetic medium lacking histidine followed by an 8-h induction in synthetic medium with galactose as a carbon source. Cells were harvested and resuspended in 0.6 ml/g lysis buffer (50 mM $NaH_2PO_4$, 300 mM NaCl, pH 8) containing EDTA-free protease inhibitors (GE Healthcare), 10 μg/ml pepstatin, 1 μg/ml antipain, and the following phosphatase inhibitors: 10 mM sodium pyrophosphate, 10 mM β-glycerophosphate, and 10 mM sodium fluoride. The cell suspension was drop-frozen in liquid nitrogen. Frozen yeast pellets were lysed in a Retsch MM301 grinding mill following the manufacturer's instructions. The ground powder was thawed, supplied with additional lysis buffer at 0.4 ml/g cells, and cleared via centrifugation. The supernatant was incubated with nickel-nitrilotriacetic acid resin (Qiagen) at 4 °C for 1 h. Bound proteins were washed with 10 mM imidazole and eluted with 250 mM imidazole. The eluted samples were dialyzed against 50 mM HEPES, pH 7.4, 100 mM NaCl, 1 mM DTT, and 10% glycerol, aliquoted, and frozen at −80 °C. CP and Blm10-CP were purified as described previously (14).

*In Vitro Protein Degradation Assay*—Dnm1 turnover was tested at 30 °C in 50 mM Tris-HCl, pH 7.5, 25 mM NaCl, 2.5 mM $MgCl_2$, 0.5 mM EDTA, 0.6% Nonidet P-40 supplemented with 350 nM $His_6$-Dnm1 in the absence of proteasomes or in the presence of 10 nM CP or 10 nM Blm10-CP. At the times indicated, aliquots were supplemented with SDS sample buffer and boiled for 3 min to stop the reaction. Dnm1 levels were visualized via SDS-PAGE and immunoblotting with anti poly-histidine antibody (Sigma). Anti-CP antibodies were from Biomol. The ECL-based chemiluminescence signals were recorded using an ImageQuant LAS 4000 mini instrument and quantified with the ImageQuant TL software.

*Detection of Programmed Cell Death*—Survival after treatment with cell death stimuli was tested as described previously (41). Briefly, WT, *blm10Δ*, *blm10ΔC3, DNM1-OE,* and *fis1Δ* (BY4741, yMS63, yMS567, yMS1058, and yMS713, respectively) cells were grown overnight in YPD medium at 30 °C. Overnight cultures were diluted to $OD_{660} = 0.2$ in YPD and incubated at 30 °C until mid-log phase was reached. Cultures were supplemented with 250 mM acetic acid and incubated for 4 h at 30 °C. Subsequently, 5-fold serial dilutions of treated and untreated cells were spotted on solid YPD medium to test for survival.

## RESULTS

*Loss of BLM10 Results in Reduced Fitness during Respiratory Growth and under Oxidative Stress*—We reported previously that *BLM10* overexpression decreases the viability of yeast cells under conditions that induce oxidative metabolism at elevated temperatures, such as growth on nonfermentable carbon sources (14). We also demonstrated that *BLM10* expression is strongly induced in response to the metabolic switch from fermentation to oxidative metabolism in yeast (19). Furthermore, increased frequency of petite colonies, indicative of impaired mitochondrial function (42) upon loss of *BLM10* in different strain backgrounds was observed (Fig. 1, *A–C*) (22). Because of their ability to ferment carbon sources, yeast cells can dispense with functional mitochondria, and thus petite strains are viable, yet growth is abolished if nonfermentable carbon sources are
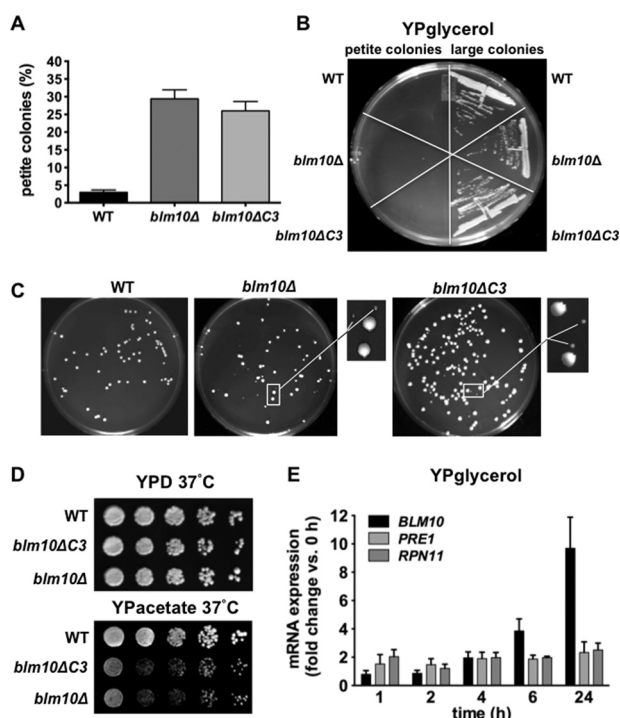
**FIGURE 1. Loss of *BLM10* results in phenotypes associated with mitochondrial dysfunction.** *A,* cells from the strains indicated were grown overnight, diluted, and spread onto YPD plates. The frequency of petite colonies in WT, *blm10Δ*, and *blm10ΔC3* strains was determined by visual inspection. The numbers of colonies counted were as follows: WT, 675; *blm10Δ*, 647; *blm10ΔC3,* 920. *B,* small and large colonies from the plates used for *A* were streaked onto plates containing the nonfermentable carbon source glycerol. *C,* representative cell spreads for the strains indicated. The size difference between normal colonies and petite colonies is highlighted in the *enlarged sections to the right. D,* serial dilutions of WT, *blm10ΔC3,* or *blm10Δ* cells were tested for growth on YPD and YP/acetate at 37 °C. *E,* expression of the genes indicated was analyzed using quantitative RT-PCR with mRNA isolated from WT yeast cells during growth in YP/glycerol at the times indicated. The means of three independent experiments are shown. $C_T$ values were normalized to *ACT1* expression levels. Values for each gene are presented relative to the 0-h time point.

used. The petite colonies in *BLM10*-deleted yeast strains are unable to grow on the nonfermentable carbon source glycerol (Fig. 1*B*) confirming that they do not contain functional mitochondria. In addition, growth of *blm10Δ* cells is impaired on the nonfermentable acetate at higher temperature (Fig. 1*C*). These observations point to a previously unidentified function of Blm10 proteasomes in the maintenance of mitochondrial function. We recently demonstrated that deletion of the last three residues of Blm10 containing the HbY*X* motif at the C terminus (*blm10ΔC3*) prevents CP binding and causes a loss-of-function phenotype (14, 19). Similar to complete *BLM10* deletion, cells expressing the CP binding-incompetent *Blm10* mutant exhibit elevated levels of colonies with dysfunctional mitochondria and a temperature-sensitive growth defect on nonfermentable carbon sources (Fig. 1, *A–C*). Thus, the role of Blm10 in the maintenance of correct mitochondrial function requires its association with and activation of the proteasome.

We hypothesized that if *BLM10* function is specifically required during respiratory growth, we might observe an increase in *BLM10* expression if cells are grown in the presence of nonfermentable carbon sources. In agreement with this hypothesis, we observed an ~10-fold induction of *BLM10* tran-

scripts during growth in medium with glycerol as a carbon source as tested via quantitative RT-PCR (Fig. 1*E, dark gray bars*). This finding is consistent with the increased expression of *BLM10* observed upon entry into oxidative metabolism or upon treating cells during logarithmic growth with the TORC1 inhibitor rapamycin (19). Genes for CP and RP subunits (*PRE1* and *RPN11*) were not up-regulated during growth on glycerol (Fig. 1*E*).

*Loss of BLM10 Leads to Reduced Respiratory Capacity and Increased Oxidative Damage of Mitochondria*—We tested the respiratory capacity of *blm10Δ* and WT cells by high resolution respirometry using an Oroboros Oxygraph-O2K, which records mitochondrial oxygen consumption. We measured respiration of WT cells and cells deleted for *BLM10* at basal level and in the presence of CCCP and TET. Addition of CCCP causes dissipates of the proton gradient across the mitochondrial membrane. The proton gradient across the mitochondrial membrane has a crucial regulatory function on the capacity of the respiratory chain complexes. Removing the membrane potential by addition of CCCP allows for the recording of maximum respiration. *blm10Δ* cells exhibited an ~40% increase in maximum respiration as compared with WT mitochondria (Fig. 2*A, left panel*). Subsequently, respiration in the presence of the ATP synthase inhibitor TET was determined, which allows for determining nonphosphorylating respiration caused by proton leakage across the inner mitochondrial membrane (LEAK flux). TET addition led to ~20% higher respiration rate in cells without Blm10 as compared with WT. From these data we calculated an *in vivo* RSV (38) and found that cells lacking Blm10 exhibit an ~60% reduction in respiratory chain activity (Fig. 2*A, right panel*). Finally, we measured the activity of aconitase in isolated mitochondria. The activity of mitochondrial aconitase is exquisitely sensitive to oxidative stress (43). We observed severely impaired mitochondrial aconitase activity in the absence of *BLM10* (Fig. 2*B*), indicative of elevated oxidative stress within the mitochondria upon loss of *BLM10*. We therefore reasoned that *Blm10* mutants might exhibit increased sensitivity during oxidative stress. When we treated cells with hydrogen peroxide or menadione, we found this hypothesis confirmed as in the absence of *BLM10* or in the presence of a CP binding-incompetent *Blm10* mutant reduced viability after oxidative stress induced by either hydrogen peroxide ($H_2O_2$) or menadione was observed (Fig. 2*C, right panels*).

*Loss of BLM10 Affects the Morphological Integrity of Mitochondria during Oxidative Stress*—Next, we investigated the structural integrity of the mitochondrial network in the absence or presence of oxidative stress. To that end, we visualized mitochondria utilizing GFP fused to cytochrome *c* oxidase subunit 4 as a reporter (39) in *blm10Δ* and WT cells in the absence or presence of $H_2O_2$. The mitochondrial morphology in untreated cells was largely comparable (Fig. 3, *right panels*). During the time course of the experiment, we also did not observe major morphological changes in WT cells after $H_2O_2$ treatment (Figs. 3, *left panels,* and 4, *A* and *B*). In *Blm10* mutants however, we observed a significant increase in mitochondrial fragmentation after incubation with $H_2O_2$ (Figs. 3, *left panels,* and 4, *A* and *B*). Approximately 50% of *blm10Δ* and
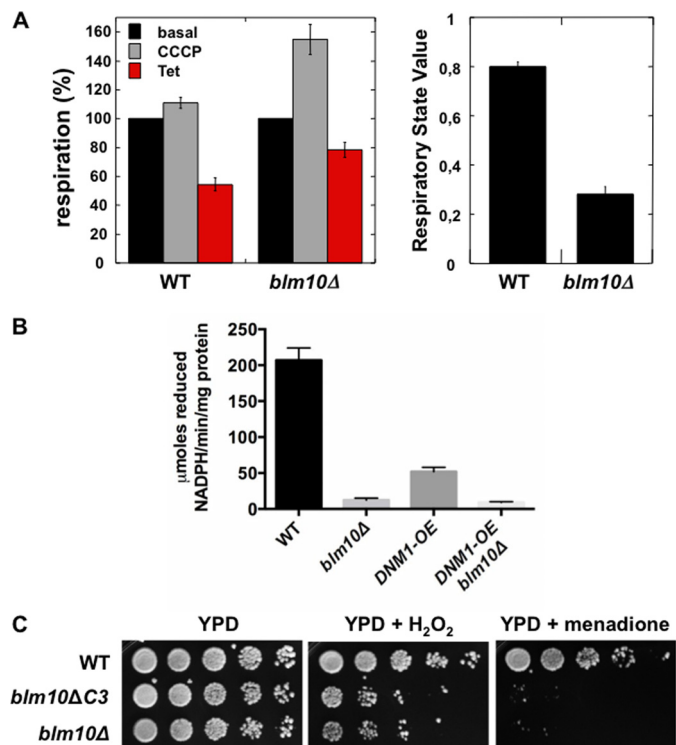
FIGURE 2. **Loss of *BLM10* results in respiratory defects and increased mitochondrial oxidative stress.** *A,* respiratory capacity of WT or *blm10Δ* cells grown in lactate was determined using an Oroboros high resolution respirometer. *Left,* basal respiration was measured in the absence of drugs. To determine maximal respiration, the uncoupling reagent CCCP was added, which dissipates the proton gradient across the mitochondrial membrane. Leak flux was analyzed in the presence of TET, an inhibitor of ATP synthase. *Right,* RSV is defined as $(JO_{basal} - JO_{TET})/(JO_{CCCP} - JO_{TET})$ and represents the percentage of stimulation of oxidative phosphorylation compared with the basal respiration capacity. *B,* aconitase activity was determined in mitochondria isolated from WT, *blm10Δ*, *DNM1-OE*, and *DNM1-OE blm10Δ* cells grown in lactate. *C,* WT, *blm10ΔC3*, or *blm10Δ* cells were treated with 10 mM $H_2O_2$ or with 300 $\mu$M menadione for 3.5 and for 1.5 h, respectively. Serial dilutions of treated and untreated cells were spotted on YPD and grown at 30 °C. *Error bars,* S.E.
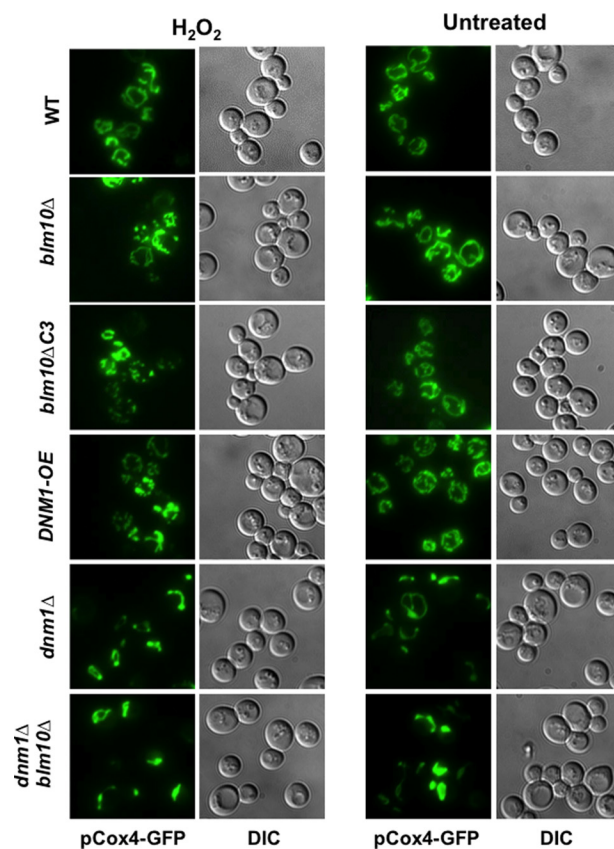
FIGURE 3. Increased mitochondrial fragmentation in *blm10Δ* cells after exposure to oxidative stress mitochondria of WT, *blm10Δ*, *blm10ΔC3*, *DNM1-OE*, *dnm1Δ*, and *blm10Δ dnm1Δ* cells were visualized using a vector expressing Cox4-GFP after treatment with 5 mM $H_2O_2$ for 4 h using live cell fluorescence microscopy (*left panels*). Untreated controls are shown in the *right panels*. Projected sequential *Z-stack* fluorescence images are presented. *DIC,* differential interference contrast.

*blm10ΔC3* cells exhibited a fragmented phenotype as compared with ~18% in the WT.

Increased mitochondrial fragmentation could be caused by increased activity of the mitochondrial fission machinery. A crucial protein, which drives the mitochondrial fission process, is the dynamin-like GTPase Dnm1 (44). We hypothesized that Blm10 proteasomes might be involved in the turnover of Dnm1 and that the increased mitochondrial fragmentation observed in *Blm10* mutants might originate from impaired Dnm1 degradation. To investigate whether elevated Dnm1 levels are sufficient to increase mitochondrial fission under oxidative stress, we treated cells overexpressing *DNM1* (*DNM1-OE*) with $H_2O_2$ and observed a similar increase in mitochondrial fragmentation as observed for *Blm10* mutants (Figs. 3, *left panels,* and 4, *A* and *B*). To explore whether Dnm1 is a key factor, which determines increased mitochondrial fission in the presence of *Blm10* mutants, we analyzed the mitochondrial morphology after $H_2O_2$ treatment in cells deleted for *DNM1* in the presence or absence of *BLM10*. In *dnm1Δ* cells, mitochondrial fission is blocked resulting in a fused mitochondrial network (Figs. 3, *right panels,* and 4*A, lower panel*) (44). Furthermore, in the absence of *DNM1* $H_2O_2$ does not trigger mitochondrial frag-

mentation, and this phenotype was not dependent on the presence of *BLM10* (Figs. 3, *left panels,* and 4, *A* and *B*). These observations suggest that the increased mitochondrial fission observed in *Blm10* mutants during oxidative stress might be caused by impaired Dnm1 turnover. This hypothesis predicts that Dnm1 overexpression should exacerbate the temperature-sensitive growth defect we observed in *Blm10* mutants. To test this, we created a strain deleted for *BLM10* and overexpressing *DNM1* (*DNM1-OE blm10Δ*). In cells overexpressing *DNM1*, deletion of *BLM10* results in a growth arrest under the same experimental conditions (Fig. 4*C*). These data corroborate the hypothesis that the temperature-sensitive growth defect of *blm10Δ* cells is related to impaired Dnm1 turnover.

As described above, we detected increased oxidative damage in mitochondria isolated from *blm10Δ* cells (Fig. 2*B*). To test whether increased Dnm1 levels could produce a similar phenotype, we measured aconitase activity in mitochondria isolated from cells overexpressing *DNM1* and observed a significant reduction. Co-deletion of *BLM10* in that strain led to additive effects (Fig. 2*B*). Finally, we tested whether overexpression of Dnm1 leads to impaired growth on nonfermentable carbon sources as observed for *Blm10* mutants. A growth defect on acetate at 37 °C was evident in cells overexpressing *DNM1*, and co-deleting *BLM10* in cells overexpressing *DNM1* led to a growth arrest (Fig. 4*C*). In summary, the phenotypic character-

**A**

| H₂O₂ treated cells (number of cells counted) | tubular (%) | linear (%) | nets (%) | fragmented (%) | large spots (%) |
|---|---|---|---|---|---|
| WT (252) | 26.59 | 23.01 | 26.19 | 18.26 | 5.95 |
| *blm10Δ* (309) | 19.74 | 16.45 | 14.5 | 43.69 | 5.61 |
| *blm10ΔC3* (184) | 4.35 | 24.46 | 18.48 | 47.83 | 4.89 |
| *DNM1-OE* (244) | 13.51 | 16.8 | 12.29 | 45.1 | 12.3 |
| *dnm1Δ* (245) | - | 26.12 | 40 | - | 33.88 |
| *blm10Δ dnm1Δ* (184) | - | 33.7 | 17.39 | - | 48.91 |

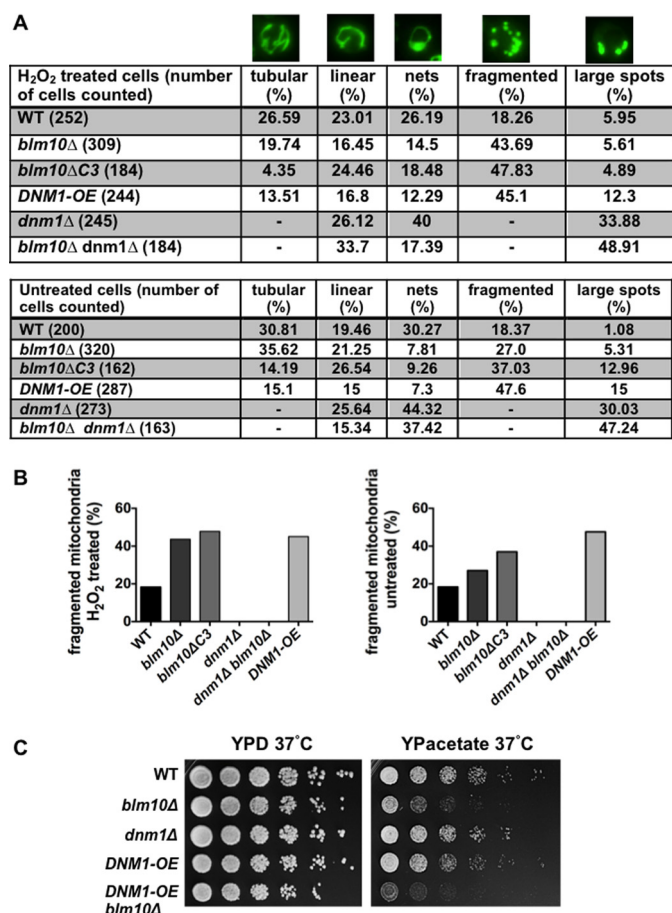| Untreated cells (number of cells counted) | tubular (%) | linear (%) | nets (%) | fragmented (%) | large spots (%) |
|---|---|---|---|---|---|
| WT (200) | 30.81 | 19.46 | 30.27 | 18.37 | 1.08 |
| *blm10Δ* (320) | 35.62 | 21.25 | 7.81 | 27.0 | 5.31 |
| *blm10ΔC3* (162) | 14.19 | 26.54 | 9.26 | 37.03 | 12.96 |
| *DNM1-OE* (287) | 15.1 | 15 | 7.3 | 47.6 | 15 |
| *dnm1Δ* (273) | - | 25.64 | 44.32 | - | 30.03 |
| *blm10Δ dnm1Δ* (163) | - | 15.34 | 37.42 | - | 47.24 |

**B**



**C**



**FIGURE 4. Mitochondrial membrane morphology in *BLM10* and *DNM1* mutants in the presence of oxidative stress.** *A,* distinct mitochondrial morphologies of the images obtained in Fig. 3 from cells incubated in the presence (*top*) or absence (*bottom*) of H₂O₂ were quantified by visual inspection. *B, bar graph* of the relative distribution of cells with fragmented mitochondria incubated in the presence (*left*) or absence (*right*) of H₂O₂ as presented in *A. C,* serially diluted overnight cultures of WT, *blm10Δ, dnm1Δ, DNM1-OE,* and *DNM1-OE blm10Δ* were spotted onto YPD and YP/acetate plates and grown at 37 °C.

istics as well as the mitochondrial structural and functional changes observed in *Blm10* mutants are phenocopied by *DNM1* overexpression.

*Abundance of Dnm1 Is Regulated by Blm10 Proteasomes—* Our results suggest that Dnm1 might be a physiological target for Blm10 proteasomes. To investigate Dnm1 abundance in *blm10Δ* cells and in cells harboring a CP binding-incompetent *Blm10* mutant, we studied the steady state levels of Dnm1 in the different growth phases in yeast. We found Dnm1 levels elevated in *blm10Δ* cells in stationary phase (Fig. 5*A*), where yeast mitochondria are known to fragment (45). Next, we tested the rate of Dnm1 turnover *in vivo* via a CHX chase assay. The addition of lethal doses of the translation inhibitor CHX blocks new synthesis. Thus, the degradation of a protein *in vivo* can be monitored (19). We examined Dnm1 levels in WT, in *Blm10* mutants, and in cells with reduced proteasome abundance through deletion of the proteasome-related transcription factor Rpn4 (1, 46). We observed impaired Dnm1 turnover in *blm10Δ, blm10ΔC3,* and in *rpn4Δ* cells (Fig. 5, *B* and *C*), suggesting that Dnm1 stability is regulated by the proteasome and involves the proteasome activator Blm10. To unambiguously
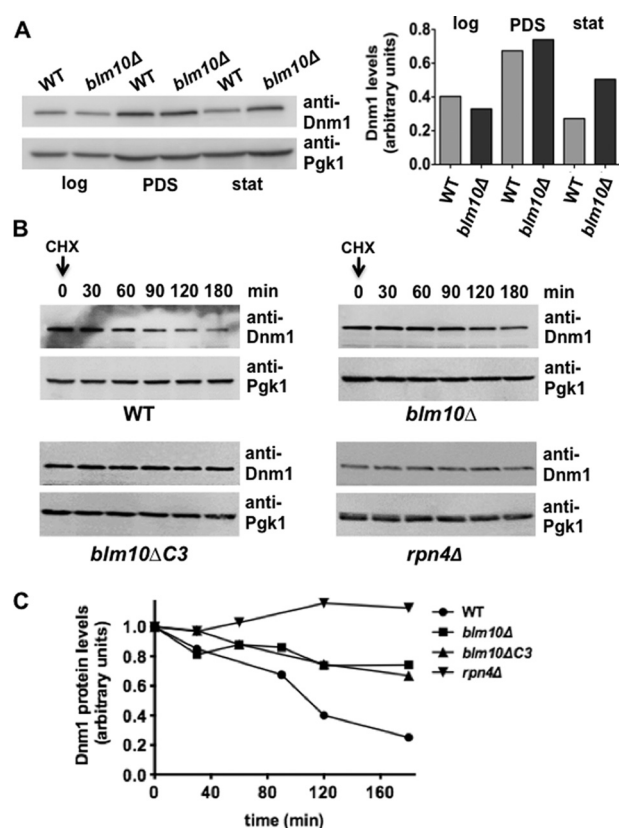
**A**



**B**



**C**



**FIGURE 5. Impaired Dnm1 turnover in *Blm10* mutant strains.** *A,* Dnm1 steady state levels in WT and *blm10Δ* strains in the three metabolic phases of yeast growth as follows: logarithmic growth phase (*log*); PDS; and stationary phase (*stat*). Equal protein amounts were subjected to SDS-PAGE followed by immunodetection with a Dnm1-specific antiserum. Immunodetection of Pgk1 was used as loading control. Chemiluminescence intensities of the band in the blots presented in *A* were recorded in an ImageQuant LAS 4000 mini system, quantified using the ImageQuant TL software and corrected for the loading control (Pgk1). The ratio of Dnm1 and Pgk1 protein levels is shown in the *left panel. B,* Dnm1 turnover was determined in WT, *blm10Δ, blm10ΔC3,* and *rpn4Δ* strains after new synthesis was blocked by 0.2 mg/ml CHX. At the time points indicated, cells were harvested and lysed, and equal protein amounts were subjected to SDS-PAGE followed by immunodetection with a Dnm1-specific antibody. An ImageQuant LAS 4000Mini Image system was used for immunodetection. PGK1 protein levels were determined with a Pgk1-specific antibody and were used as loading control. *C,* chemiluminescence intensities of the band in the blots presented in *A* were recorded in an ImageQuant LAS 4000 mini system, quantified using the ImageQuant TL software, and corrected for the loading control (Pgk1).

determine the impact of Blm10 on proteasome-mediated Dnm1 degradation, we purified Dnm1 and endogenous Blm10 proteasome core particle complexes (Blm10-CP) from yeast and tested Dnm1 turnover in a purified system (Fig. 6 (*A* and *B*)). In the absence of CP or Blm10-CP, the level of Dnm1 remains largely unchanged during the time course of the experiment. Addition of CP in the absence of Blm10 led to a slight reduction in Dnm1. Blm10-CP complexes, however, rapidly degraded Dnm1. ATP or ubiquitination of Dnm1 was not required for turnover of the protein. These data demonstrate that Blm10 induces proteasome-mediated Dnm1 turnover.

*Blm10 Activates Dnm1 Degradation, but Does Not Affect the Abundance of Other Fission Components nor Fzo1—*To investigate whether other components of the fission machinery are regulated by proteasomal degradation, we tested the turnover of Fis1 and Mdv1 *in vivo*. Within the time frame of our experi-
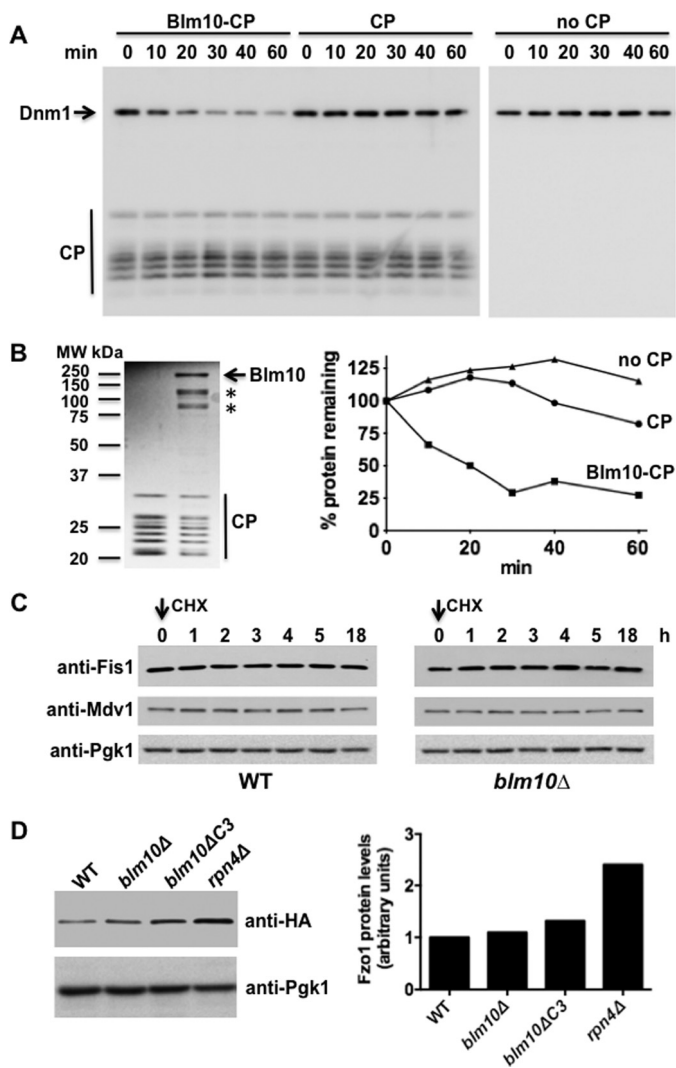
FIGURE 6. **Dnm1 is degraded by Blm10 proteasomes *in vitro*.** *A,* Dnm1 degradation was investigated in a purified system in the presence of 10 nM Blm10-CP (*left lanes*), CP (*middle lanes*), or in the absence of proteasomes (*right lanes*). Dnm1 detection was achieved via an N-terminal His$_6$ tag using an anti-polyhistidine antibody. The same membranes were tested for CP levels using an anti-CP antibody (*lower signals*). *B, left panel,* 0.7 μg of CP or Blm10-CP used in *A* were separated via SDS-PAGE and stained with Coomassie Blue. *, Blm10 degradation products. *Right panel,* chemiluminescence intensities of the bands shown in the blots presented in *A* were recorded in an ImageQuant LAS 4000 mini system and quantified using the ImageQuant TL software. *C, in vivo* turnover of the fission proteins Fis1 and Mdv1 was determined as in Fig. 5*A* with Fis1- and Mdv1-specific antibodies after blocking new synthesis with lethal doses of the ribosome inhibitor CHX. *D,* Fzo1-HA levels were analyzed in normalized lysates in the strains indicated using an HA-specific antibody. Chemiluminescence intensities of the bands shown in the blots presented in the *left panel* were recorded in an ImageQuant LAS 4000 mini system, quantified using the ImageQuant TL software, and corrected for the loading control (Pgk1) (*right panel*).

ments, the level of both proteins remained unchanged (Fig. 6*C*); thus, proteasomal degradation of mitochondrial fission proteins appears to be restricted to Dnm1. Rather than from elevated mitochondrial fission, increased fragmentation might also originate from reduced activity of the fusion machinery. The yeast mitofusin is regulated through proteasomal degradation and abrogated function of the UPS leads to stabilization of mitofusins and reduced fragmentation of the mitochondrial network (47). If Blm10 would affect the fusion machinery, we would expect decreased abundance of Fzo1. In contrast, for
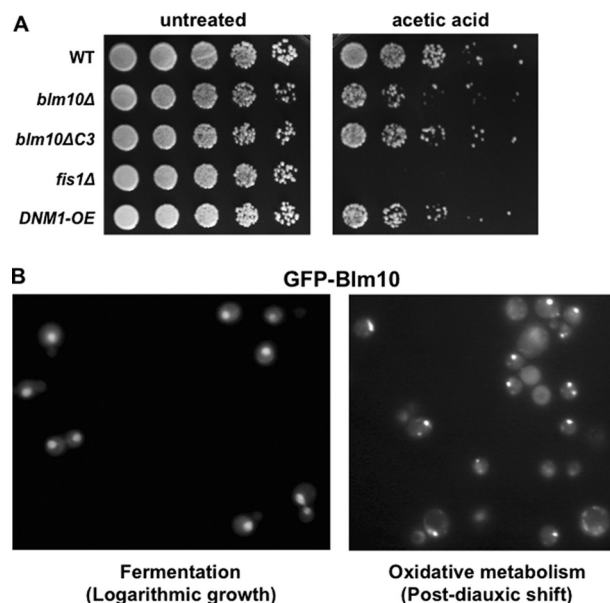


FIGURE 7. **Decreased viability of *Blm10* mutants in the presence of high doses of acetic acid.** *A,* after treatment of WT, *blm10Δ*, *blm10ΔC3*, *DNM1-OE*, and *fis1Δ* with 250 mM acetic acid for 4 h, treated and untreated cells were serially diluted and spotted on YPD to test for survival. *B,* to monitor Blm10 localization, a plasmid containing the *BLM10* gene under its endogenous promoter was N-terminally tagged with GFP and transformed in a *BLM10* deletion strain. GFP fluorescence was analyzed in living cells in logarithmically growing cells (*left panel*) and after the diauxic shift (*right panel*).

*rpn4Δ* cells, however, which exhibit elevated Fzo1 levels, Fzo1 abundance is unchanged in *Blm10* mutants (Fig. 6*D*). These data suggest that the impact of Blm10 on mitochondrial dynamics is specific to Dnm1.

*Loss of BLM10 Confers Hypersensitivity to Death Stimuli*—A conserved function for Dnm1/Drp1 proteins is their involvement in programmed cell death (28, 48). In response to a death stimulus such as high concentrations of acetic acid, the yeast mitochondrial fragment and this process are mediated by Dnm1 (48). Overexpression of Dnm1 reduces the viability after a death stimulus (Fig. 7*A*, *right panel*) (48). We therefore hypothesized that *blm10Δ* cells might exhibit reduced viability after acetic acid treatment. When cells lacking *BLM10* were treated with 250 mM acetic acid, they inhibit reduced viability (Fig. 7*A*, *right panel*), which we attribute to reduced turnover of Dnm1. *fis1Δ* cells, which are known to be exquisitely sensitive to death stimuli, were used as controls (48). These observations are consistent with the reduced viability of *Blm10* mutants after treatment with H$_2$O$_2$ or menadione (Fig. 2*C*), both of which are known to induce programmed cell death in yeast.

*Nutrient-dependent Blm10 Nuclear Export*—During logarithmic growth, Blm10 is localized predominantly to the nucleus (10, 16), consistent with the mostly nuclear localization of yeast proteasomes under those conditions (49). A nuclear localization of Blm10, however, is not easily reconciled with the degradation of a cytoplasmic target such as Dnm1. Recently, it was reported that proteasomes exit the yeast nucleus when cells pass the diauxic shift (50), and reports in the fission yeast *Schizosaccharomyces pombe* demonstrate a cytoplasmic localization of the proteasome in G$_0$ cells (51). Because our data indicate that Blm10 is involved in Dnm1 turnover in the cytoplasm, we hypothesized that Blm10 might also exit the nucleus

after the diauxic shift. We thus monitored the fluorescence of a GFP-tagged version of Blm10 in log and PDS phase and observed that, similarly to the proteasome, the predominantly nuclear localization of Blm10 is lost in PDS (Fig. 7*B*). In some cells, we observed a focal localization of Blm10 in the cytoplasm consistent with the localization pattern for the proteasome, which forms discrete cytosolic foci termed proteasome storage granules during starvation or upon the switch to oxidative metabolism (50).

## DISCUSSION

Mitochondria are dynamic organelles that continuously fuse and divide, and the machineries that govern mitochondrial fission and fusion are conserved from yeast to human (52). The dynamic nature of the mitochondrial network is essential for aligning the capacity of the organelle with the energetic and metabolic requirements of eukaryotic cells (52). Mitochondrial network adaptations are especially evident in the sperm flagellum, where fused mitochondria are wrapped around the base of the flagellum (53), or during mitosis, where the mitochondrial network is highly fragmented (54). Regulated mitochondrial fission and fusion also play a role in organelle transport, *e.g.* in neurons, in quality control of mitochondria, and in mitochondrial inheritance during cell division. In addition, mitochondrial fragmentation is linked to the execution of programmed cell death programs (55). Thus, proteins involved in regulating mitochondrial fission and fusion are crucial factors for the health of eukaryotic cells. Here, we report that Blm10 proteasome-mediated proteolysis of the fission protein Dnm1 impacts mitochondrial morphology and is required for correct mitochondrial function under normal growth conditions and under conditions that induce mitochondrial stress.

Dnm1 and its human ortholog Drp1 are large dynamin-related GTPases (39, 44) that cooperate with adaptor proteins to promote mitochondrial fission. Dnm1/Drp1 proteins share the classical dynamin property to assemble into oligomeric structures (56, 57). They are mechanochemical enzymes, which use their GTPase activity to drive membrane fission (58). It is thought that mitochondrial fragmentation provides a quality control mechanism for the organelle by isolating defective, depolarized mitochondria, which facilitates their removal from the cell via mitophagy (28, 59). This hypothesis is supported by reports demonstrating that knockdown of Drp1 in mammalian cells leads to impaired mitochondrial function and loss of mitochondrial DNA (26). Loss of Drp1 in *Caenorhabditis elegans* results in embryonic lethality (60), and mutations in human Drp1 are associated with a lethal birth syndrome characterized by microcephaly, abnormal brain development, optic atrophy, and persistent lactic acidemia (61). Drp1/Dnm1-mediated mitochondrial fragmentation is furthermore an early event during apoptosis and programmed cell death (35, 48).

Many mechanistic details have been identified that regulate Drp1 function in mammalian cells. They can be grouped into two main categories, post-translational modification and regulated turnover (33, 62). Several kinases and phosphatases are known to impact Drp1 activity and recruitment to the mitochondria (62). Furthermore, ubiquitination and sumoylation regulate Drp1 function. Sumoylation stabilizes Drp1, presum-
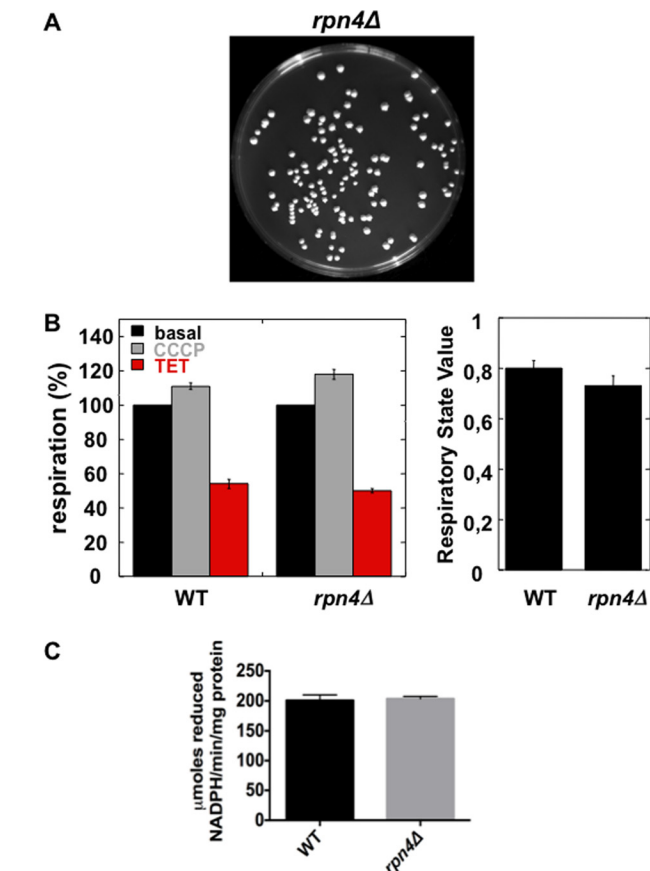


FIGURE 8. **Loss of Rpn4 does not result in increased frequency of petite colonies, respiratory defects, or increased mitochondrial oxidative stress.** *A*, representative spread of *rpn4Δ* cells revealing a lack of petite colonies. *B*, respiratory capacity of WT and *rpn4Δ* cells was determined as described in the legend to Fig. 2*A*. *C*, mitochondrial aconitase activity was determined in mitochondria isolated from WT and *rpn4Δ* cells as described in the legend to Fig. 2*B*. *Error bars*, S.E.

ably through an antagonistic effect of sumoylation and ubiquitination (63). The ubiquitin E3 ligase MARCH5/MITOL polyubiquitinates Drp1 but does not trigger Drp1 degradation (64). Polyubiquitination by the E3 ligase Parkin, however, regulates proteasomal degradation of Drp1 (65). Ubiquitin-independent Blm10 proteasome-mediated degradation of Dnm1 adds an additional control mechanism to this list. At present, it is unknown whether the impact of Blm10 on fusion is conserved in mammals. Interestingly, loss of PA200, the mammalian ortholog of Blm10, in mice results in reduced male fertility caused by impaired spermatogenesis (20), and PA200 expression is strongly elevated in testes (9, 15). Mitochondria in sperm cells reveal a specific adaptation to the increased energy demand of mobile cells, *i.e.* a highly fused mitochondrial network (53). It is therefore tempting to speculate that the increased PA200 levels in testes are required for increased degradation of Drp1 and thus to down-regulate the fission process.

Mitochondrial morphology is determined by the balanced activity of the fission and fusion machineries. We demonstrate here that Blm10 proteasome activators mediate the turnover of Dnm1 to counteract mitochondrial fission, but they have no impact on fusion. However, a recent study demonstrated that proteasome-mediated degradation of the mitochondrial fusion protein Mfn2 promotes stress-induced mitochondrial fission
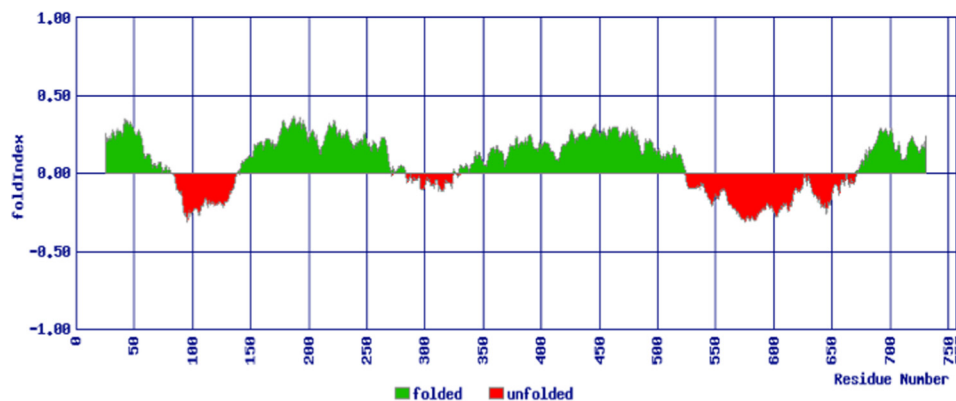
FIGURE 9. **Prediction of intrinsically unstructured regions in the Blm10-CP target Dnm1.** The protein sequence of Dnm1 was analyzed using the Fold-Index algorithm (66).

and apoptosis in mammals (47), and in yeast, UPS-mediated regulation of the Mfn2 ortholog Fzo1 impacts mitochondrial dynamics (32, 34). Thus, proteasomal degradation can promote fission through increased degradation of Mfn2/Fzo1 or it can inhibit fission by reducing Dnm1/Drp1 levels as concluded from the data presented here. The decision whether fission or fusion is promoted by proteasome-mediated degradation must rely on additional signals. Proteasomal turnover of Mfn2 is induced by JNK-mediated phosphorylation in the presence of doxorubicin (47). Whether phosphorylation of Dnm1/Drp1 is involved in regulating proteasome-mediated turnover of Dnm1/Drp1 is not known.

Based on the data reported here, we propose an additional mechanism for differential regulation of fission and fusion via proteasomal degradation, differential regulation via different proteasome subpopulations. We propose that proteasomal regulation of mitochondrial fusion is executed by the 26 S proteasome through degradation of Mfn2/Fzo1, whereas Dnm1/Drp1 degradation is mediated by Blm10/PA200 proteasomes. A specific role for Blm10 in regulating mitochondrial fission is supported by several observations. We did not observe impaired Fzo1 degradation in cells lacking *BLM10*. *BLM10* expression is up-regulated under conditions, which induce oxidative metabolism resulting in increased oxidative damage to mitochondria. Furthermore, even though Dnm1 is stabilized in *rpn4Δ* cells (Fig. 5*A*), which are characterized by a general reduction in proteasome capacity (46), these cells do not exhibit impaired mitochondrial function or generate petite colonies at high frequency, nor do they exhibit increased oxidative damage to mitochondria (Fig. 8). Thus, reduced proteasome activity primarily impacts mitochondrial fusion, whereas loss of *BLM10* specifically enhances fission.

Cells with a CP binding-incompetent *Blm10* mutant, lacking the last three residues of the 240-kDa protein, exhibit impaired Dnm1 degradation similar to complete loss of the protein and show the same phenotypic characteristics as *blm10Δ* cells. These data suggest that the impact of Blm10 on Dnm1 turnover requires CP binding and activation. Mechanistically, it is still unclear how Blm10 promotes proteasomal substrate degradation. A co-crystal structure of reconstituted Blm10-CP complexes showed that Blm10 binding to the CP results in an at least partially open gate (22). The conformations of the N-ter-

minal residues of four of the α subunits are superimposable with the open gate conformation of PA26-CP complexes (5). The remaining three N termini could not be (19) from the closed gate conformation. Our previous reports showed that Blm10 mediates proteasomal turnover of the transcription factor Sfp1, and *in vitro* Blm10 accelerates CP-mediated degradation of Tau-441 (14) indicating that the structural changes of the CP gate upon Blm10 binding are sufficient to promote protein entry and turnover. Both Sfp1 and Tau are characterized by large unstructured domains. We also found that ATP or ubiquitination is not required for Blm10-mediated proteasome activation. These observations led to a model in which Blm10 might specifically promote the degradation of unstructured proteins. This hypothesis is supported by a recent study demonstrating Blm10- and PA200-mediated degradation of core histones. Sfp1 and Tau histones also contain large unstructured domains (15). Using an algorithm, which predicts unfolded domains in proteins (66), we detected a relatively large unfolded region of ~150 amino acids in Dnm1 (Fig. 9), and we propose that this region might provide a recognition motif for Blm10 proteasome-mediated degradation.

**REFERENCES**
1. Finley, D. (2009) Recognition and processing of ubiquitin-protein conjugates by the proteasome. *Annu. Rev. Biochem.* **78,** 477–513
2. Vabulas, R. M., and Hartl, F. U. (2005) Protein synthesis upon acute nutrient restriction relies on proteasome function. *Science* **310,** 1960–1963
3. Groll, M., Ditzel, L., Löwe, J., Stock, D., Bochtler, M., Bartunik, H. D., and Huber, R. (1997) Structure of 20S proteasome from yeast at 2.4 Å resolution. *Nature* **386,** 463–471
4. Groll, M., Bajorek, M., Köhler, A., Moroder, L., Rubin, D. M., Huber, R., Glickman, M. H., and Finley, D. (2000) A gated channel into the proteasome core particle. *Nat. Struct. Biol.* **7,** 1062–1067
5. Stadtmueller, B. M., and Hill, C. P. (2011) Proteasome activators. *Mol. Cell* **41,** 8–19
6. Demartino, G. N., and Gillette, T. G. (2007) Proteasomes: machines for all reasons. *Cell* **129,** 659–662
7. Glickman, M. H., Rubin, D. M., Fu, H., Larsen, C. N., Coux, O., Wefes, I., Pfeifer, G., Cjeka, Z., Vierstra, R., Baumeister, W., Fried, V., and Finley, D. (1999) Functional analysis of the proteasome regulatory particle. *Mol. Biol. Rep.* **26,** 21–28

8. Strehl, B., Seifert, U., Krüger, E., Heink, S., Kuckelkorn, U., and Kloetzel, P. M. (2005) Interferon-γ, the functional plasticity of the ubiquitin-proteasome system, and MHC class I antigen processing. *Immunol. Rev.* **207,** 19–30

9. Ustrell, V., Hoffman, L., Pratt, G., and Rechsteiner, M. (2002) PA200, a nuclear proteasome activator involved in DNA repair. *EMBO J.* **21,** 3516–3525

10. Schmidt, M., Haas, W., Crosas, B., Santamaria, P. G., Gygi, S. P., Walz, T., and Finley, D. (2005) The HEAT repeat protein Blm10 regulates the yeast proteasome by capping the core particle. *Nat. Struct. Mol. Biol.* **12,** 294–303

11. Li, X., Amazit, L., Long, W., Lonard, D. M., Monaco, J. J., and O'Malley, B. W. (2007) Ubiquitin- and ATP-independent proteolytic turnover of p21 by the REGγ-proteasome pathway. *Mol. Cell* **26,** 831–842

12. Chen, X., Barton, L. F., Chi, Y., Clurman, B. E., and Roberts, J. M. (2007) Ubiquitin-independent degradation of cell-cycle inhibitors by the REGγ proteasome. *Mol. Cell* **26,** 843–852

13. Iwanczyk, J., Sadre-Bazzaz, K., Ferrell, K., Kondrashkina, E., Formosa, T., Hill, C. P., and Ortega, J. (2006) Structure of the Blm10–20 S proteasome complex by cryo-electron microscopy. Insights into the mechanism of activation of mature yeast proteasomes. *J. Mol. Biol.* **363,** 648–659

14. Dange, T., Smith, D., Noy, T., Rommel, P. C., Jurzitza, L., Cordero, R. J., Legendre, A., Finley, D., Goldberg, A. L., and Schmidt, M. (2011) Blm10 protein promotes proteasomal substrate turnover by an active gating mechanism. *J. Biol. Chem.* **286,** 42830–42839

15. Qian, M. X., Pang, Y., Liu, C. H., Haratake, K., Du, B. Y., Ji, D. Y., Wang, G. F., Zhu, Q. Q., Song, W., Yu, Y., Zhang, X. X., Huang, H. T., Miao, S., Chen, L. B., Zhang, Z. H., Liang, Y. N., Liu, S., Cha, H., Yang, D., Zhai, Y., Komatsu, T., Tsuruta, F., Li, H., Cao, C., Li, W., Li, G. H., Cheng, Y., Chiba, T., Wang, L., Goldberg, A. L., Shen, Y., and Qiu, X. B. (2013) Acetylation-mediated proteasomal degradation of core histones during DNA repair and spermatogenesis. *Cell* **153,** 1012–1024

16. Fehlker, M., Wendler, P., Lehmann, A., and Enenkel, C. (2003) Blm3 is part of nascent proteasomes and is involved in a late stage of nuclear proteasome assembly. *EMBO Rep.* **4,** 959–963

17. Marques, A. J., Glanemann, C., Ramos, P. C., and Dohmen, R. J. (2007) The C-terminal extension of the β7 subunit and activator complexes stabilize nascent 20 S proteasomes and promote their maturation. *J. Biol. Chem.* **282,** 34869–34876

18. Blickwedehl, J., Agarwal, M., Seong, C., Pandita, R. K., Melendy, T., Sung, P., Pandita, T. K., and Bangia, N. (2008) Role for proteasome activator PA200 and postglutamyl proteasome activity in genomic stability. *Proc. Natl. Acad. Sci. U.S.A.* **105,** 16165–16170

19. Lopez, A. D., Tar, K., Krügel, U., Dange, T., Ros, I. G., and Schmidt, M. (2011) Proteasomal degradation of Sfp1 contributes to the repression of ribosome biogenesis during starvation and is mediated by the proteasome activator Blm10. *Mol. Biol. Cell* **22,** 528–540

20. Khor, B., Bredemeyer, A. L., Huang, C. Y., Turnbull, I. R., Evans, R., Maggi, L. B., Jr., White, J. M., Walker, L. M., Carnes, K., Hess, R. A., and Sleckman, B. P. (2006) Proteasome activator PA200 is required for normal spermatogenesis. *Mol. Cell. Biol.* **26,** 2999–3007

21. Blickwedehl, J., Olejniczak, S., Cummings, R., Sarvaiya, N., Mantilla, A., Chanan-Khan, A., Pandita, T. K., Schmidt, M., Thompson, C. B., and Bangia, N. (2012) The proteasome activator PA200 regulates tumor cell responsiveness to glutamine and resistance to ionizing radiation. *Mol. Cancer Res.* **10,** 937–944

22. Sadre-Bazzaz, K., Whitby, F. G., Robinson, H., Formosa, T., and Hill, C. P. (2010) Structure of a Blm10 complex reveals common mechanisms for proteasome binding and gate opening. *Mol. Cell* **37,** 728–735

23. Fisk, H. A., and Yaffe, M. P. (1999) A role for ubiquitination in mitochondrial inheritance in *Saccharomyces cerevisiae*. *J. Cell Biol.* **145,** 1199–1208

24. Radke, S., Chander, H., Schäfer, P., Meiss, G., Krüger, R., Schulz, J. B., and Germain, D. (2008) Mitochondrial protein quality control by the proteasome involves ubiquitination and the protease Omi. *J. Biol. Chem.* **283,** 12681–12685

25. Heo, J. M., Livnat-Levanon, N., Taylor, E. B., Jones, K. T., Dephoure, N., Ring, J., Xie, J., Brodsky, J. L., Madeo, F., Gygi, S. P., Ashrafi, K., Glickman, M. H., and Rutter, J. (2010) A stress-responsive system for mitochondrial

26. Parone, P. A., Da Cruz, S., Tondera, D., Mattenberger, Y., James, D. I., Maechler, P., Barja, F., and Martinou, J. C. (2008) Preventing mitochondrial fission impairs mitochondrial function and leads to loss of mitochondrial DNA. *PLoS One* **3,** e3257

27. Rambold, A. S., Kostelecky, B., Elia, N., and Lippincott-Schwartz, J. (2011) Tubular network formation protects mitochondria from autophagosomal degradation during nutrient starvation. *Proc. Natl. Acad. Sci. U.S.A.* **108,** 10190–10195

28. Mao, K., Wang, K., Liu, X., and Klionsky, D. J. (2013) The scaffold protein Atg11 recruits fission machinery to drive selective mitochondria degradation by autophagy. *Dev. Cell* **26,** 9–18

29. Altmann, K., and Westermann, B. (2005) Role of essential genes in mitochondrial morphogenesis in *Saccharomyces cerevisiae*. *Mol. Biol. Cell* **16,** 5410–5417

30. Rinaldi, T., Hofmann, L., Gambadoro, A., Cossard, R., Livnat-Levanon, N., Glickman, M. H., Frontali, L., and Delahodde, A. (2008) Dissection of the carboxyl-terminal domain of the proteasomal subunit Rpn11 in maintenance of mitochondrial structure and function. *Mol. Biol. Cell* **19,** 1022–1031

31. Joshi, K. K., Chen, L., Torres, N., Tournier, V., and Madura, K. (2011) A proteasome assembly defect in rpn3 mutants is associated with Rpn11 instability and increased sensitivity to stress. *J. Mol. Biol.* **410,** 383–399

32. Cohen, M. M., Leboucher, G. P., Livnat-Levanon, N., Glickman, M. H., and Weissman, A. M. (2008) Ubiquitin-proteasome-dependent degradation of a mitofusin, a critical regulator of mitochondrial fusion. *Mol. Biol. Cell* **19,** 2457–2464

33. Chang, C. R., and Blackstone, C. (2010) Dynamic regulation of mitochondrial fission through modification of the dynamin-related protein Drp1. *Ann. N. Y. Acad. Sci.* **1201,** 34–39

34. Anton, F., Dittmar, G., Langer, T., and Escobar-Henriques, M. (2013) Two deubiquitylases act on mitofusin and regulate mitochondrial fusion along independent pathways. *Mol. Cell* **49,** 487–498

35. Suen, D. F., Norris, K. L., and Youle, R. J. (2008) Mitochondrial dynamics and apoptosis. *Genes Dev.* **22,** 1577–1590

36. Brachmann, C. B., Davies, A., Cost, G. J., Caputo, E., Li, J., Hieter, P., and Boeke, J. D. (1998) Designer deletion strains derived from *Saccharomyces cerevisiae* S288C: a useful set of strains and plasmids for PCR-mediated gene disruption and other applications. *Yeast* **14,** 115–132

37. Goldstein, A. L., and McCusker, J. H. (1999) Three new dominant drug resistance cassettes for gene disruption in *Saccharomyces cerevisiae*. *Yeast* **15,** 1541–1553

38. Dejean, L., Beauvoit, B., Guérin, B., and Rigoulet, M. (2000) Growth of the yeast *Saccharomyces cerevisiae* on a nonfermentable substrate: control of energetic yield by the amount of mitochondria. *Biochim. Biophys. Acta* **1457,** 45–56

39. Sesaki, H., and Jensen, R. E. (1999) Division *versus* fusion: Dnm1p and Fzo1p antagonistically regulate mitochondrial shape. *J. Cell Biol.* **147,** 699–706

40. Jansen, G., Wu, C., Schade, B., Thomas, D. Y., and Whiteway, M. (2005) Drag&Drop cloning in yeast. *Gene* **344,** 43–51

41. Teng, X., and Hardwick, J. M. (2009) Reliable method for detection of programmed cell death in yeast. *Methods Mol. Biol.* **559,** 335–342

42. Ferguson, L. R., and von Borstel, R. C. (1992) Induction of the cytoplasmic 'petite' mutation by chemical and physical agents in *Saccharomyces cerevisiae*. *Mutat. Res.* **265,** 103–148

43. Gardner, P. R., Raineri, I., Epstein, L. B., and White, C. W. (1995) Superoxide radical and iron modulate aconitase activity in mammalian cells. *J. Biol. Chem.* **270,** 13399–13405

44. Bleazard, W., McCaffery, J. M., King, E. J., Bale, S., Mozdy, A., Tieu, Q., Nunnari, J., and Shaw, J. M. (1999) The dynamin-related GTPase Dnm1 regulates mitochondrial fission in yeast. *Nat. Cell Biol.* **1,** 298–304

45. Braun, R. J., and Westermann, B. (2011) Mitochondrial dynamics in yeast cell death and aging. *Biochem. Soc. Trans.* **39,** 1520–1526

46. Kruegel, U., Robison, B., Dange, T., Kahlert, G., Delaney, J. R., Kotireddy, S., Tsuchiya, M., Tsuchiyama, S., Murakami, C. J., Schleit, J., Sutphin, G., Carr, D., Tar, K., Dittmar, G., Kaeberlein, M., Kennedy, B. K., and Schmidt, M. (2011) Elevated proteasome capacity extends replicative lifespan in

The reference numbered 8 continues from the previous page; reference 25 continues: "protein degradation. *Mol. Cell* **40,** 465–480"

*Saccharomyces cerevisiae. PLoS Genet.* **7**, e1002253

47. Leboucher, G. P., Tsai, Y. C., Yang, M., Shaw, K. C., Zhou, M., Veenstra, T. D., Glickman, M. H., and Weissman, A. M. (2012) Stress-induced phosphorylation and proteasomal degradation of mitofusin 2 facilitates mitochondrial fragmentation and apoptosis. *Mol. Cell* **47**, 547–557

48. Fannjiang, Y., Cheng, W. C., Lee, S. J., Qi, B., Pevsner, J., McCaffery, J. M., Hill, R. B., Basañez, G., and Hardwick, J. M. (2004) Mitochondrial fission proteins regulate programmed cell death in yeast. *Genes Dev.* **18**, 2785–2797

49. Russell, S. J., Steger, K. A., and Johnston, S. A. (1999) Subcellular localization, stoichiometry, and protein levels of 26 S proteasome subunits in yeast. *J. Biol. Chem.* **274**, 21943–21952

50. Laporte, D., Salin, B., Daignan-Fornier, B., and Sagot, I. (2008) Reversible cytoplasmic localization of the proteasome in quiescent yeast cells. *J. Cell Biol.* **181**, 737–745

51. Takeda, K., and Yanagida, M. (2010) In quiescence of fission yeast, autophagy and the proteasome collaborate for mitochondrial maintenance and longevity. *Autophagy* **6**, 564–565

52. Okamoto, K., and Shaw, J. M. (2005) Mitochondrial morphology and dynamics in yeast and multicellular eukaryotes. *Annu. Rev. Genet.* **39**, 503–536

53. Sutovsky, P., Navara, C. S., and Schatten, G. (1996) Fate of the sperm mitochondria, and the incorporation, conversion, and disassembly of the sperm tail structures during bovine fertilization. *Biol. Reprod.* **55**, 1195–1205

54. Taguchi, N., Ishihara, N., Jofuku, A., Oka, T., and Mihara, K. (2007) Mitotic phosphorylation of dynamin-related GTPase Drp1 participates in mitochondrial fission. *J. Biol. Chem.* **282**, 11521–11529

55. Otera, H., Ishihara, N., and Mihara, K. (2013) New insights into the function and regulation of mitochondrial fission. *Biochim. Biophys. Acta* **1833**, 1256–1268

56. Koirala, S., Guo, Q., Kalia, R., Bui, H. T., Eckert, D. M., Frost, A., and Shaw, J. M. (2013) Interchangeable adaptors regulate mitochondrial dynamin assembly for membrane scission. *Proc. Natl. Acad. Sci. U.S.A.* **110**, E1342–E1351

57. Tieu, Q., Okreglak, V., Naylor, K., and Nunnari, J. (2002) The WD repeat protein, Mdv1p, functions as a molecular adaptor by interacting with Dnm1p and Fis1p during mitochondrial fission. *J. Cell Biol.* **158**, 445–452

58. Fukushima, N. H., Brisch, E., Keegan, B. R., Bleazard, W., and Shaw, J. M. (2001) The GTPase effector domain sequence of the Dnm1p GTPase regulates self-assembly and controls a rate-limiting step in mitochondrial fission. *Mol. Biol. Cell* **12**, 2756–2766

59. Twig, G., and Shirihai, O. S. (2011) The interplay between mitochondrial dynamics and mitophagy. *Antioxid. Redox Signal.* **14**, 1939–1951

60. Labrousse, A. M., Zappaterra, M. D., Rube, D. A., and van der Bliek, A. M. (1999) *C. elegans* dynamin-related protein DRP-1 controls severing of the mitochondrial outer membrane. *Mol. Cell* **4**, 815–826

61. Waterham, H. R., Koster, J., van Roermund, C. W., Mooyer, P. A., Wanders, R. J., and Leonard, J. V. (2007) A lethal defect of mitochondrial and peroxisomal fission. *N. Engl. J. Med.* **356**, 1736–1741

62. Elgass, K., Pakay, J., Ryan, M. T., and Palmer, C. S. (2013) Recent advances into the understanding of mitochondrial fission. *Biochim. Biophys. Acta* **1833**, 150–161

63. Zunino, R., Schauss, A., Rippstein, P., Andrade-Navarro, M., and McBride, H. M. (2007) The SUMO protease SENP5 is required to maintain mitochondrial morphology and function. *J. Cell Sci.* **120**, 1178–1188

64. Karbowski, M., Neutzner, A., and Youle, R. J. (2007) The mitochondrial E3 ubiquitin ligase MARCH5 is required for Drp1 dependent mitochondrial division. *J. Cell Biol.* **178**, 71–84

65. Wang, H., Song, P., Du, L., Tian, W., Yue, W., Liu, M., Li, D., Wang, B., Zhu, Y., Cao, C., Zhou, J., and Chen, Q. (2011) Parkin ubiquitinates Drp1 for proteasome-dependent degradation: Implication of dysregulated mitochondrial dynamics in Parkinson disease. *J. Biol. Chem.* **286**, 11649–11658

66. Prilusky, J., Felder, C. E., Zeev-Ben-Mordehai, T., Rydberg, E. H., Man, O., Beckmann, J. S., Silman, I., and Sussman, J. L. (2005) FoldIndex: A simple tool to predict whether a given protein sequence is intrinsically unfolded. *Bioinformatics* **21**, 3435–3438

**Proteasomes Associated with the Blm10 Activator Protein Antagonize Mitochondrial Fission through Degradation of the Fission Protein Dnm1**

Krisztina Tar, Thomas Dange, Ciyu Yang, Yanhua Yao, Anne-Laure Bulteau, Elena Fernandez Salcedo, Stephen Braigen, Frederic Bouillaud, Daniel Finley and Marion Schmidt

Access the most updated version of this article at doi: 10.1074/jbc.M114.554105

Alerts:
- When this article is cited
- When a correction for this article is posted

Click here to choose from all of JBC's e-mail alerts

This article cites 66 references, 31 of which can be accessed free at
http://www.jbc.org/content/289/17/12145.full.html#ref-list-1